Journal of Power Sources 239 (2013) 1–8

Contents lists available at SciVerse ScienceDirect

Journal of Power Sources

journal homepage: www.elsevier.com/locate/jpowsour

In search of an appropriate ionic liquid as electrolyte for macroporous manganese oxide film electrochemistry

Tânia M. Benedetti, Vinicius R. Gonçales, Susana I. Córdoba de Torresi, Roberto M. Torresi*

Instituto de Química, Universidade de São Paulo, CP 26077, 05513-970 São Paulo-SP, Brazil

HIGHLIGHTS

- There is no difference among the surface areas films of differing pore sizes.
- Capacitances are due both surface charge compensation and intercalation processes.
- The best cycling performance was observed for Li^+/[BMMI][Tf_2N] electrolyte.
- Oxide dissolution occurs in Li^+/[Et_2OMMI][Tf_2N] and Li^+/[BMMI][BF_4].

ARTICLE INFO

Article history:
Received 14 January 2013
Received in revised form
6 March 2013
Accepted 11 March 2013
Available online 28 March 2013

Keywords:
Manganese oxide
Ionic liquid
Porous films
Electrochemical capacitor
Template assisted electrodeposition

ABSTRACT

Macroporous manganese oxide films were produced via template-assisted electrodeposition methodology employing polystyrene spheres with different diameters as template, thereby producing films with different pore sizes. The obtained films were true casts of the template(s) employed, as evidenced by Field Emission Scanning Electron Microscopy. The influence of pore size on capacitive behavior was assessed by cyclic voltammetry experiments in conventional propylene carbonate/$LiClO_4$. Besides the influence of pore size, four different ionic liquids (ILs) were studied as electrolytes, showing that the physico–chemical nature of IL strongly affects the capacitive behavior of macroporous manganese oxide films, particularly in terms of stability throughout successive charge/discharge cycles. Optimal performance was obtained using 1-butyl-2,3-dimethylimidazolium bis(trifluoromethanesulfonyl)imide ([BMMI][Tf_2N]), in which a constant increase in capacitance was observed for the first 700 charge/discharge cycles. This capacitance remained constant, at least until the 1,000 cycle, and was higher than the capacitance achieved using conventional organic solvents. Moreover, the electrochemical window obtained using [BMMI][Tf_2N] was widened (from 0.9 V to 1.5 V), corresponding to a significant gain (up to 75%) in terms of energy density. Thus, the development of electrochemical capacitors may significantly benefit from macroporous manganese oxide film electrochemistry employing ionic liquids as electrolytes.

1. Introduction

Because of their advantageous properties, such as low flammability, negligible vapor pressure and high ionic conductivity [1], ionic liquids (ILs) have been extensively studied for use as electrolytes in electrochemical devices such as lithium batteries [2–6]. In addition to these advantageous characteristics, ILs are stable throughout a wide electrochemical window, which is extremely important given that energy and power density are strongly affected by cell voltage.

Another advantage of ILs is their potential to combine several cations and anions, thus making it possible to modify the ILs' properties according to the desired particular applications [7]. However, in spite of attempts to understand the relationship between structure(s) and properties, it is still a considerable challenge to determine which IL is the best suited electrolyte for a given system.

Some studies have demonstrated the use of ILs as electrolytes in electrochemical capacitors [8–10]. In contrast to lithium batteries, in which charge compensation is primarily obtained via the Li^+ ions provided by the salt added to the IL, in electrochemical capacitors the ions from the IL itself can take part in this process, which typically occurs at the surface of the electroactive material. Recently, Li and co-workers have demonstrated that adding small ions such as Na^+, H^+ and Cl^-, thereby providing electroactive sites

* Corresponding author. Tel.: +55 11 30919194; fax: +55 11 38155640.
E-mail address: rtorresi@iq.usp.br (R.M. Torresi).

0378-7753/$ – see front matter © 2013 Elsevier B.V. All rights reserved.
http://dx.doi.org/10.1016/j.jpowsour.2013.03.075

Table 1
Prepared ionic liquids and their physico–chemical properties at 25 °C.

Ionic liquid	Full name	σ/mS cm^{-1}	η/mPa s	Ref.
[BMMI][Tf_2N]	1-Butyl-2,3-dimethylimidazolium bis(trifluoromethanesulfonyl)imide	1.6	93	[23]
[Et_2OMMI][Tf_2N]	1-Ethoxyethyl-2,3-dimethylimidazolium bis(trifluoromethanesulfonyl)imide	2.3	67	[24]
[BMP][Tf_2N]	N-n-Butyl-N-methylpiperidinium bis(trifluoromethanesulfonyl)imide	1.2	183	[23]
[BMMI][BF_4]	1-Butyl-2,3-dimethylimidazolium tetrafluoroborate	0.9	515	[25]

that are unavailable via the more voluminous ions in the IL, can improve the capacitance in systems containing manganese oxide as the electrode material and an IL as the electrolyte [11].

Due to its high theoretical capacitance and low cost, manganese oxide was widely studied for use in supercapacitor [12,13]. However, due its relatively poor experimental capacitance (compared to theoretical values), most recent work involved synthesizing materials with increased surface areas to increase their electrochemical performance [14–17]. Among others strategies, electrodeposition of films around a colloidal crystal template was suggested as a good alternative for producing macroporous materials with high surface areas [18–20]. Initial studies regarding template-assisted electrodeposition of macroporous manganese oxide employed polystyrene spheres was done, and the resulting film was electrochemically characterized using aqueous electrolytes [21,22]. However, only one sphere size was used in these studies; therefore, there was no investigation or discussion regarding the effect(s) of pore size on electrochemical performance.

Based on these assumptions, the goals of the present contribution are both to study the influence of pore size on capacitive behavior of manganese oxide films as well as the influence of physico–chemical nature of different ionic liquids on the electrochemical performance of manganese oxide macroporous films.

2. Experimental

2.1. Syntheses of ILs

Ionic liquids were prepared and purified according to procedures described in previously published studies. The procedures used are shown in Table 1 and their cations and anions structures are showed in Fig. 1.

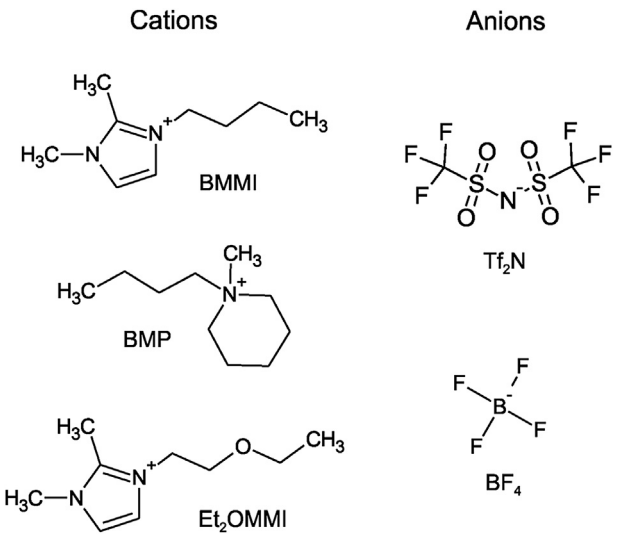

Fig. 1. Structures of cations and anions of ionic liquids.

In general, after the imidazole compound was reacted with the longer chain bromide to give the IL cation bromide, an ionic exchange reaction with the desired anion was performed. After synthesis, the water content of each IL was measured via Karl-Fischer titration with a Metrohm – 831 KF Coulometer; a value between 200 and 1000 ppm was obtained in all cases.

2.2. Preparation of manganese-oxide macroporous films

A scheme presenting the preparation of manganese oxide macroporous films is presented in Fig. 2.

2.2.1. Assembly of polystyrene spheres over a gold substrate

Aqueous suspensions (10% (w/w)) of polystyrene nanospheres with differing diameters (300, 460, 600 and 800 nm) were diluted to 0.5% using Triton-X 100 aqueous solutions of differing concentrations (depending on the sphere sizes used). Three 10-μL aliquots of the obtained suspensions were placed (via micropipette) on the substrate, which consisted of the gold surface of a 6 MHz, AT-cut, overtone polished, piezoelectric quartz crystal (Valpey-Fisher) with a diameter of 25 mm and a piezo-active electrode area of 0.31 cm^2 (integral sensitivity factor, $K = 6.45 \times 10^7$ cm^2 Hz g^{-1} [26]. The surfactant used was important to ensure homogeneous assemblage of the polystyrene spheres over the substrate. After each 10 μL aliquot application and prior to the subsequent application, the gold surface was slowly dried at room temperature in a saturated-humidity atmosphere. After the last aliquot was applied and the surface was dry, the deposits obtained were submitted to thermal treatment at 100 °C for varying times, depending on the particular sphere size employed. The Triton-X 100 concentrations and thermal treatment times for each sphere size are given in Table 2.

2.2.2. Electrodeposition of manganese oxide around the polystyrene spheres

Manganese-oxide films were obtained via oxidation (at a constant voltage) of 2 mmol L^{-1} $MnSO_4$ + 50 mmol L^{-1} $LiClO_4$ aqueous solution (as electrolyte) [27]. Immediately prior to electrodeposition, the substrate containing the polystyrene template was immersed in the electrodeposition solution for 1 h to completely swell the voids among spheres within the electrode. Electrodeposition was obtained by applying 1 V (vs. an Ag/AgCl/KCl_{sat} reference electrode) and increasing the charge until it reached 180 mC cm^{-2} (using an Autolab PGSTAT 30 potentiostat). After the electrochemical process was complete, the substrate containing the MnO_2 deposit was rinsed with deionized water and dried with N_2 gas.

To remove the polystyrene template, the electrode was immersed in tetrahydrofuran, which was then stirred for 45 min, after which the electrode was washed with ethanol and dried under N_2 flow. The mass of the electrodeposited material was obtained by measuring the resonance frequency of the quartz crystal before the deposition of polystyrene spheres and after their removal. Frequency shifts were measured using a Stanford Research Systems Model SR620 instrument connected to an oscillating circuit (serial mode) and a microcomputer for data acquisition. Complete removal of polystyrene spheres from the manganese oxide film was confirmed via FESEM using a Jeol microscope, model JSM-7401F.

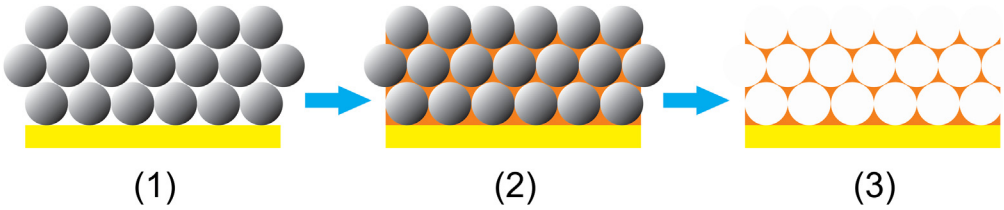

Fig. 2. Representation of growth of manganese oxide around polystyrene spheres template. (1) assembly of PS spheres; (2) manganese oxide electrodeposition; (3) removal of PS spheres.

2.3. Manganese oxide powder characterization

Manganese-oxide powder was obtained using the same electrochemical conditions employed to produce macroporous films but in the absence of spheres templates. The electrodeposited material was scratched from the electrode and characterized by X-ray diffraction and thermogravimetric analyses using Rigaku Miniflex equipment and TA instruments (TGA2950 equipment), respectively.

2.4. Morphologic characterization of macroporous films

The films obtained were analyzed via field emission scanning electron microscopy (FESEM). For thickness measurements, the substrate containing the macroporous film was immersed in liquid nitrogen, fractured and placed in a vertical position to obtain cross-sectional images.

2.5. Electrochemical characterization

Macroporous films with different pore sizes were electrochemically characterized via cyclic voltammetry using a Autolab PGSTAT 30 potentiostat. An organic solvent and several IL electrolytes were used, as described in Table 3. For comparison, electrochemical characterization was also performed in [BMMI][Tf_2N] without the addition of lithium salt.

All experiments were performed in a three electrode cell using an Ag wire and a Pt mesh as the pseudo-reference and counter electrodes, respectively. Voltammetric studies of ILs containing ferrocene (as the internal reference) were previously performed to define the potential window. The electrochemical cell was kept inside a glove box (MBraun) under argon atmosphere with O_2 and H_2O contents below 1 ppm during measurements.

3. Results and discussion

3.1. Characterization of manganese oxide powder

The oxide powder was characterized using XRD and TGA. The results are disclosed in Fig. 3. According to the XRD data previously reported by Nakayama et al. [27], after thermal treatment at 80 °C for 3 h and then X-ray photoelectron spectroscopy (XPS), the manganese oxide obtained via the present methodology possesses a birnessite structure and its molecular formula is $Li_{0.35}Mn^{3+}_{0.35}Mn^{4+}_{0.65}O_2 \cdot 1H_2O$. In the present study, no preliminary thermal treatment was performed, which explains the amorphous material observed via XRD (Fig. 3a). The unique peak obtained at approximately 37° is ascribed to the glass substrate over which the manganese oxide powder was deposited for the measurements. Regions 1 and 2 in the TGA graph (Fig. 3b) are due to losses of physically and chemically bonded water, respectively [28], corresponding to a mass loss of approximately 27%. This value is higher than the mass of water lost (17%) under the experimental conditions of the previous work. This difference in the mass of water lost likely results from the absence of thermal treatment in the present work. Subsequent mass losses occur when the manganese oxide structure changes to Mn_2O_3 and Mn_3O_4 [28].

3.2. Assembly of polystyrene spheres over gold substrate and the electrodeposition of manganese oxide

The conditions under which polystyrene spheres are assembled are of great importance with regard to achieving a suitable template for subsequent electrodeposition [29–31]. Based on the hydrophobic/hydrophilic nature of the substrate and on the size the polystyrene spheres employed, the surfactant concentration must be tuned to achieve uniform templates [32]. Whether a good template for electrodeposition is obtained also depends on the thermal treatment time. Thermal treatment at slightly above glass-transition temperature causes the formation of linkages among nanospheres, thereby avoiding their detachment during the subsequent step in which the substrate is immersed in the electrodeposition solution.

To determine the mass of the electrodeposited manganese oxide films, the resonance frequency of the quartz crystal was measured (using the QCM) both before the template was assembled and after its removal with THF. The frequency shifts measured were converted to mass values using the Sauerbrey equation [33]. Regardless of the sphere diameter(s) used, the masses of the films were always around 100 μg cm^{-2}. Fig. 4 presents FESEM images of the different films. It is extremely important to control charge deposition during macroporous-film syntheses using the methodology developed herein. If the charge deposition is too high, the material deposition

Table 2
Triton-X 100 concentration and thermal treatment times employed for polystyrene nanospheres of differing diameters.

Nanosphere diameters (Nm)	Triton-X 100 concentration (mol L^{-1})	Thermal treatment time (hours)
300	10^{-7}	1
460	10^{-6}	4
600	10^{-4}	4
800	10^{-4}	4

Table 3
Electrolytes used for electrochemical characterization of macroporous manganese oxide films.

Electrolyte	Composition
Li^+/PC	$LiClO_4$ 0.5 mol L^{-1} in propylene carbonate
Li^+/[BMMI][Tf_2N]	$LiTf_2N$ 0.5 mol L^{-1} in [BMMI][Tf_2N]
Li^+/[BMMI][BF_4]	$LiBF_4$ 0.5 mol L^{-1} in [BMMI][BF_4]
Li^+/[EtO(CH_2)$_2$MMI][Tf_2N]	$LiTf_2N$ 0.5 mol L^{-1} in [EtO(CH_2)$_2$MMI][Tf_2N]
Li^+/[BMP][Tf_2N]	$LiTf_2N$ 0.5 mol L^{-1} in [BMP][Tf_2N]

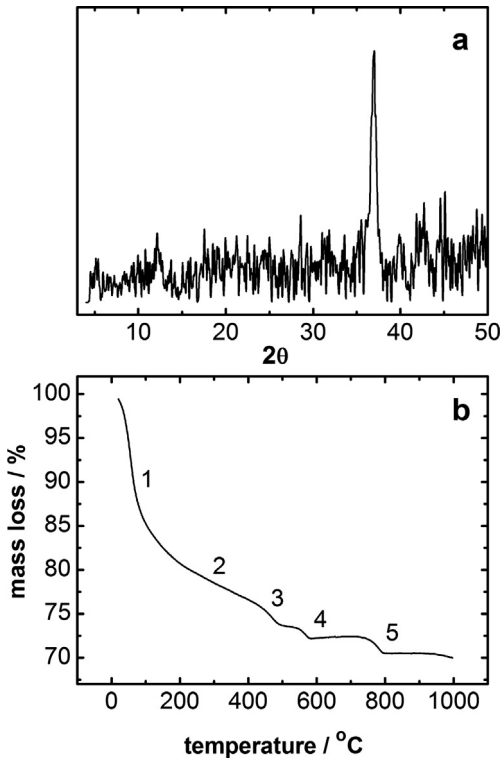

Fig. 3. (a) XRD and (b) TGA of manganese oxide powder.

will cover the template, causing blockage of electrolyte access to pores. For the present system, a suitable charge of 180 mC cm^{-2} was determined via FESEM analyses of films obtained using different charge deposition values. By monitoring the suitable charge, it was possible to obtain macroporous films of manganese oxide with pore sizes approximately equal to the diameters of the spheres employed as the template(s). The expanded image (inset in Fig. 4b) shows that the pores are interconnected throughout the film area and thickness and that spandrels (triangular gaps that appear in the film walls, depending on interaction(s) between material precursors and polystyrene spheres) are absent [34] This feature is extremely important because the connection among the pores guarantees access of the electrolyte (through the pores) to the entire film (without defects), thereby improving the material's electrical conductivity.

The distance between two adjacent pores - i.e., the thickness of the manganese oxide wall between two adjacent pores - was measured for films with different pore sizes. At least 30 measurements were obtained for each film, and the average values were compiled in Fig. 5 and the bars represent the standard deviation in distance between two adjacent pores in the 30 measurements; this variation was approximately 20% in all cases. As expected, the graph indicates that the wall between two adjacent pores increases with increasing pore diameter.

Film thicknesses were measured by "cross-section" using FESEM. At least 25 measurements were obtained for each sample. Fig. 6 shows a FESEM image of a film containing 600 nm pores (Fig. 6a) and presents the average thickness as a function of pore diameter (Fig. 5b). The standard deviation bars assigned to each macroporous film thickness value are relatively constant for all pore sizes, varying between 10 and 20% of the average value. Fig. 6b indicates a tendency toward increasing thickness with increasing pore size. Considering that independent on the polystyrene spheres' diameter, the volume available for oxide deposition is the same in all cases (the polystyrene spheres always occupy approximately 48% of the total volume), it is reasonable to conclude that the thickness is also the same (in all cases) once equivalent amounts of material are deposited. Thus, the slight increase in film thickness observed with increasing sphere size can most likely be

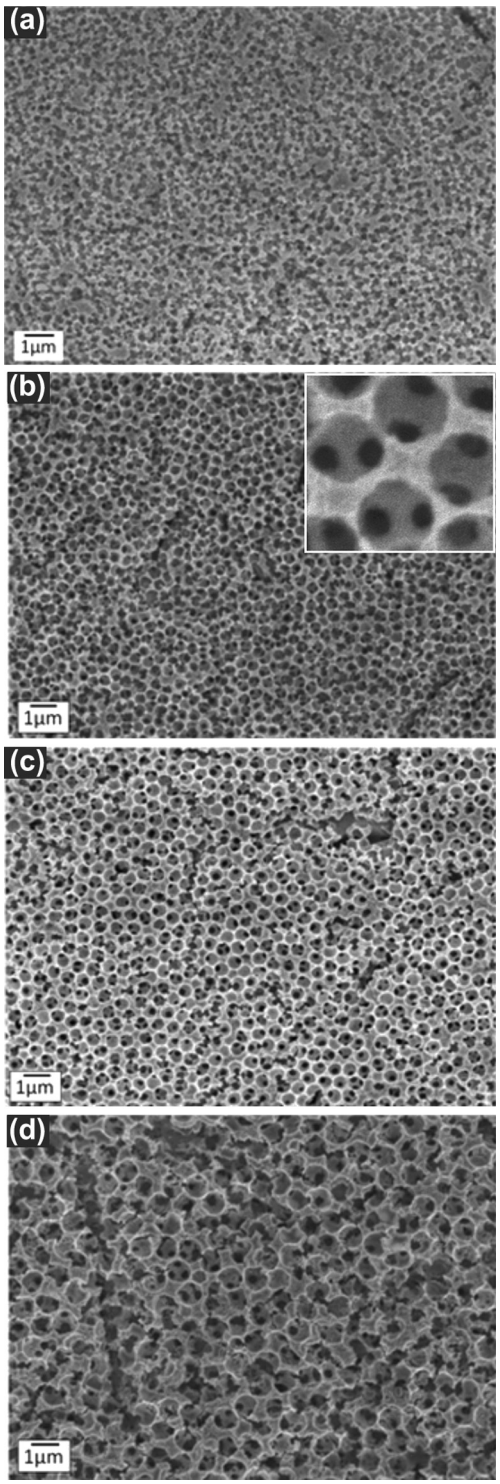

Fig. 4. FESEM images of manganese oxide films obtained through electrodeposition over templates containing polystyrene spheres with the following diameters: 300 nm (a), 460 nm (b), 600 nm (c) and 800 nm (d). Applied potential = 1 V; Reference electrode = $Ag/AgCl/KCl_{sat}$; Counter electrode = Pt mesh; and electrolyte = 5 mmol L^{-1} $MnSO_4$ + 50 mmol L^{-1} $LiClO_4$.

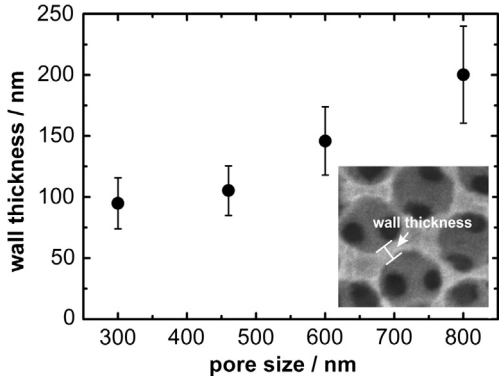

Fig. 5. Distance between two adjacent pores as a function of film pore size.

attributed to differences in manganese oxide density when it is deposited around the polystyrene template or over material that has already been deposited in the voids (given that the former is more compact than manganese oxide deposited over itself).

The surface area of macroporous films can be estimated based on equation (1) [19,35]:

$$f = n\pi\sqrt{\frac{4}{3}} \quad (1)$$

where f is the enhancement factor with respect to the massive film and n is the film thickness/pore size ratio. Calculated n and f values are disclosed in Table 4. These values clearly show that once the film with pores of 300 nm is excluded, there is virtually no difference among the surface areas of macroporous films of differing pore sizes.

3.3. Electrochemical characterization

First, the influence of pore size on electrochemical performance was investigated by cyclic voltammetry in organic-solvent-based electrolyte (Supplementary material, Figs. 1s, 2s, 3s and 4s). For each macroporous film with different pore sizes, capacitance values as a function of scan rate were calculated using equation (2), and the results were compiled in Fig. 7.

$$C = \frac{Q}{EW} \quad (2)$$

where Q is the discharge charge calculated via integration of the negative-current-as-a-function-of-time curve, EW is the potential window, usually it is shown C normalized by the mass of deposited manganese oxide. The data obtained demonstrate that, independent of pore size, the capacitance continuously decreases with an increasing scan rate (Fig. 7a). As previously observed for manganese oxide [36], this behavior is consistent with systems with capacitances that are determined by surface charge compensation as well as by intercalation processes, the latter of which are affected by the scan rate. When the surface charge compensation is the only (or the predominant) process involved, as is the case for manganese oxide macroporous films obtained via oxidation of $KMnO_4$ in aqueous electrolyte containing lithium salt (previously studied and reported by this laboratory) [22], the scan rate has little to no influence. The pronounced decrease in capacitance with increasing scan rate observed in the present work indicates that the main process contributing to the capacitance involves the intercalation of ions into the manganese oxide structure.

Table 4
The n and f factors calculated for macroporous films with different pore sizes.

Pore size/nm	n	f
300	5.5 ± 0.8	20 ± 3
460	3.9 ± 0.7	14 ± 2
600	3.4 ± 0.4	12 ± 1
800	3.3 ± 0.6	12 ± 2

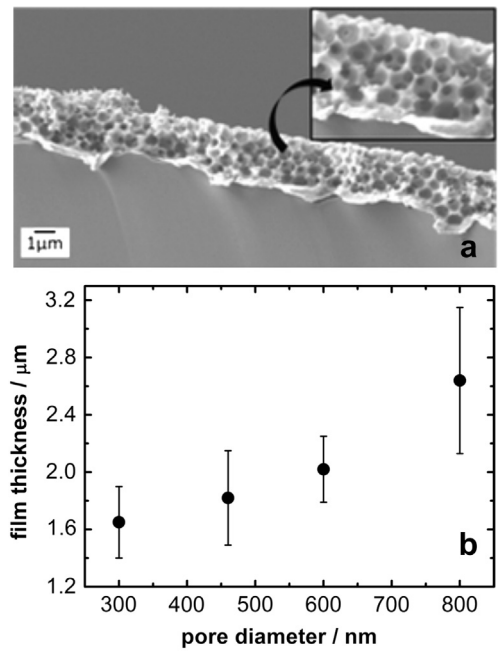

Fig. 6. (a) Cross-sectional image taken from a 600-nm (pore size) manganese oxide film; (b) film thickness as a function of pore size.

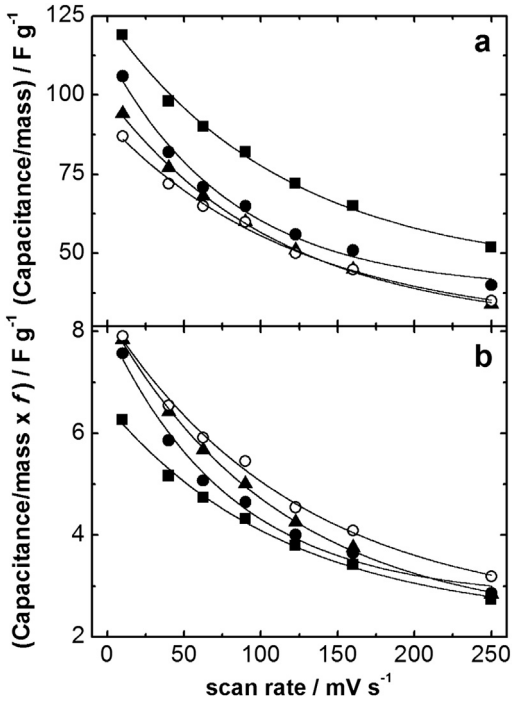

Fig. 7. Initial discharge capacitance (a) and capacitance normalized with f (b) as a function of the scan rate for manganese oxide macroporous films of differing pore sizes. Internal reference = Fc/Fc^+; counter electrode = Pt mesh; Electrolyte = Li^+/PC; 300 nm (■), 460 nm (●), 600 nm (▲) and 800 nm (○).

In addition to the effect of scan rate on capacitance, the results presented in Fig. 7a show that with the exception of the 300-nm macroporous film, capacitance increases with decreasing pore size only at low scan rates. These observations can be explained as follows. As shown in Table 4, the surface areas are similar for macroporous films with 460, 600 and 800 nm when they all have the same values of f and n. In addition, as shown in Fig. 4, the distance between two adjacent pores increases with increasing pore size. Based on this observation, one can assume that for the same surface areas, pore size will have no effect on capacitance at high scan rates, when the charge compensation process is mainly superficial. At low scan rates, intercalation through the manganese oxide structure becomes more important because intercalation is negatively affected by the increase in wall thickness associated with increasing pore size. The effect of the higher surface area of the 300-nm macroporous film is clearly observed in that the capacitance values are higher than those of the other macroporous films in all range of scan rates studied. In fact, if the capacitance values are normalized with respect to f (Fig. 6b), the values at scan rates as high as 250 mV s^{-1} are the same, independent of pore size. With decreasing scan rate, the normalized values for the 300-nm film become increasingly lower than those for the other films, supporting the tendency toward an increasing intercalation-process effect (once both superficial and intercalation contributions are divided by the factor f). However, only the superficial contribution is actually affected by surface area, as indicated by the lower value of C/f, regardless of how high the intercalation contribution becomes.

To study the electrolytic behavior of the different ILs considered herein, films with 460-nm pore diameters were used. Propylene carbonate-based electrolyte was used as a reference. Cyclic voltammetry was performed at 0.04 V s^{-1}, and the results are compiled in Fig. 8. With the exception of the macroporous film in Li^+/[BMMI][Tf_2N], which presented defined oxidation/reduction peaks in addition to capacitive behavior, all the voltammograms exhibited a predominantly near-rectangular shape. In previous work reported by Nam et al. [37], voltammograms of thin manganese oxide films obtained by electrochemical oxidation of $MnSO_4$ presented defined oxidation and reduction current peaks when performed in Li^+/PC, while a typical rectangular voltammogram shape was observed when aqueous KCl solution was used. Thus, it appears that the electrochemical behavior of thin manganese oxide films depends on the electrolyte used. In the Nam case, the difference was attributed to more facile and reversible Li^+ intercalation (compared to K^+ from the aqueous electrolyte). When lithium salt is dissolved in ionic liquids, Li^+ ions form ionic aggregates with ionic liquid anions, and the number and nature of these aggregates depends on the ionic liquid structure [24]. On this basis, the presence of redox peaks in voltammograms obtained for macroporous films in Li^+/[BMMI][Tf_2N] can be explained by better diffusivity (through the manganese oxide film) of the ionic aggregate formed in this ionic liquid.

The electrochemical stabilities of systems containing different electrolytes were determined using cyclic voltammetry. The discharge capacitance as a function of the number of cycles is presented in Fig. 9. The results clearly show that depending on the electrolyte employed, the capacitance values trend differently with cycling. When Li^+/PC or Li^+/[BMP][Tf_2N] are used, the capacitance decreases abruptly within the first 10 cycles, after which it increases, reaching a maximum value at the 20th or 40th cycle, respectively. Beyond this, the capacitance maintains a constant decrease until at least the 1,000th cycle, achieving 40% and 57% of the initial capacitance for the IL and for the organic solvent-based electrolyte, respectively. Although similar behaviors were observed for both electrolytes, the system containing the Li^+/PC electrolyte exhibited a higher initial capacitance as well as greater capacitance retention. The worst performances were observed for Li^+/[Et_2OMMI][Tf_2N] and Li^+/[BMMI][BF_4] electrolytes, in which capacitance values decreased drastically to values close to zero after 200 and 50 cycles, respectively. In these electrolytes, dissolution of manganese oxide into the electrolyte was observed visually. The best performance was observed for the system containing Li^+/[BMMI][Tf_2N], where a constant increase in capacitance value was observed until the 700th cycle, after which it achieved the highest value among all electrolytes investigated and remained constant until at least the 1,000th cycle.

These results deserve further consideration based on electrolyte properties and voltammetric behavior. For the systems containing Li^+/[BMP][Tf_2N] and Li^+/PC electrolytes, the initial capacitance decay can be associated with irreversible faradaic reactions. In fact, the broad current peaks observed in the first cycles (Fig. 8, full green square and full red triangle) that can be associated with faradaic reactions disappear after a few cycles (results not shown). The subsequent increase in capacitance is most likely related to an increase in macroporous film wettability, after which the subsequent fall in capacitance (with continued cycling) is most likely caused by film passivation or dissolution, which persists at least until the 1,000th cycle. The poor performance of Li^+/[Et_2OMMI][Tf_2N] and Li^+/[BMMI][BF_4] electrolytes is clearly due to manganese oxide dissolution, which was visible to the naked eye after only a

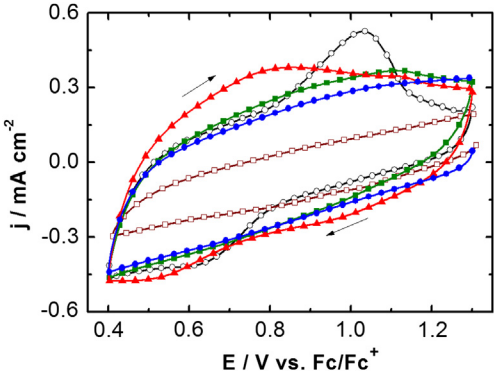

Fig. 8. Cyclic voltammogram of 460-nm (pore diameter) manganese oxide film in different electrolytes. Counter-electrode = Pt mesh; internal reference = Fc/Fc^+; scan rate = 0.04 V s^{-1}; and electrolytes = (—○—) Li^+/[BMMI][Tf_2N], (—□—) Li^+/[BMMI][BF_4], (—■—) Li^+/[BMP][Tf_2N], (—●—) Li^+/[Et_2OMMI][Tf_2N] and (—▲—) Li^+/PC.

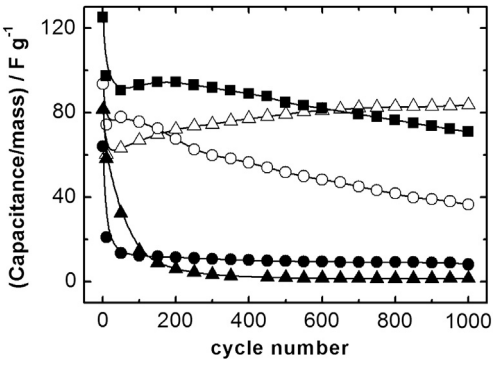

Fig. 9. Discharge capacitance as a function of cycle number. Macroporous film pore size = 460 nm; counter-electrode = Pt mesh; internal reference = Fc/Fc^+; scan rate = 0.04 V s^{-1}; electrolyte = (■) Li/PC, (○) Li/[BMP][Tf_2N], (▲) Li/[Et_2OMMI][Tf_2N], (△) Li/[BMMI][Tf_2N] and (●) Li/[BMMI][BF_4].

few cycles. When Mn^{4+} is reduced to Mn^{3+}, the following reaction can occur:

$$2Mn^{3+} \rightarrow Mn^{4+} + Mn^{2+} \quad (3)$$

The product Mn^{2+} is soluble in the electrolyte. This reaction is favored when H^+ traces are present in the electrolyte [38,39]. Given that [BMMI][BF_4] is prepared from HBF_4 and is a hydrophilic IL, it is likely that proton traces are present that can cause the dissolution of manganese oxide when this IL is employed as an electrolyte. However, dissolution in [Et_2OMMI][Tf_2N] is most likely caused by the presence of an ether chain in the IL cation. These ether chains could coordinate with Mn^{2+} ions and form stable complexes with chelating compounds [40]. The ether chains from different IL cations can most likely form structures similar to crown ethers, thereby stabilizing Mn^{2+} in solution.

In terms of capacitance retention, the best performance was observed when Li^+/[BMMI][Tf_2N] was used as the electrolyte. This behavior can be attributed to (1) increased wettability with cycling as well as (2) lower solubility of electrode material in the electrolyte. In fact, after 600 charging/discharging cycles, the capacitance achieved higher values than those obtained with the organic solvent system. Clearly, the use of manganese oxide in electrochemical systems is severely limited by issues involving its dissolution [41], which is obviously more pronounced when nanostructures of high surface films are employed. Early studies have shown that this problem can be solved, or at least minimized, by using additives in the electrolyte [42] or via recovery using electroactive nanoparticles [43]. The results presented herein indicate that it is also possible to eliminate, or minimize, the dissolution of electrode material by employing a suitable IL as the electrolyte.

Initial discharge capacitances, calculated from charge obtained from the first cycle of the correspondent voltammograms, vary as follows: Li^+/PC > Li^+/[BMP][Tf_2N] > Li^+/[Et_2OMMI][Tf_2N] > Li^+/[BMMI][Tf_2N] ~ Li^+/[BMMI][BF_4]. Considering that the capacitance follows the ionic conductivity/viscosity of ILs (see Table 1), Li^+/[Et_2OMMI][Tf_2N] should exhibit the highest capacitance value among all the ILs investigated and Li^+/[BMMI][Tf_2N] should exhibit a better performance than either Li^+/[BMP][Tf_2N] or Li^+/[BMMI][BF_4]. However, according to the results in Fig. 9, the film takes longer to wet in [BMMI][Tf_2N] compared to other ILs, which may explain its lower initial capacitance in [BMMI][Tf_2N]. However, for ILs containing ether chains, film dissolution likely occurs at the beginning of the experiment, causing lower capacitance values.

Based on its better performance, Li^+/[BMMI][Tf_2N] was chosen as the electrolyte for experiments investigating the influence of lithium salt additives on electrochemical performance/capacitance. The results are summarized in Fig. 10. In both pure ILs and mixtures with lithium salt, the capacitance is observed to decrease with increasing scan rate, providing evidence that an intercalation process is occurring in the IL. From 10 mV s^{-1}–250 mV s^{-1}, the capacitance decreases to 61% in Li^+/[BMMI][Tf_2N], similar to the behavior observed in Li^+/PC (62% – Fig. 7). However, the capacitance is significantly lower when lithium salt is absent because then only the voluminous ions from the ionic liquid are taking part in the charge compensation process. The difference in capacitance values is significant, even at scan rates as high as 250 mV s^{-1}, which is an important result with regard to the applicability of the methods herein to the development of electrochemical capacitors.

Compared to aqueous electrolytes, the wide electrochemical window in which both [BMMI][Tf_2N] and PC are stable should allow the employment of larger operational voltages, which can contribute to increases energy densities. To verify this hypothesis, the operational electrochemical window was increased to 1.5 V (from −0.5 to 1.0 V vs. Ag). The results obtained for the 800 nm (pore size) macroporous film are summarized in Fig. 11 as an example. This specific potential window was chosen based on manganese oxide oxidation/reduction behavior, once increasing the working electrochemical window did not significantly increase the capacitance. As shown by the voltammograms obtained with reduced potential windows (Fig. 8), the systems present predominant capacitive behavior, with broad oxidation/reduction peaks. Similar profiles were obtained for macroporous films with different pore sizes in both electrolytes (results not shown). Although the capacitance increases were not significant, increasing the potential window offers greater advantages with regard to energy density once the potential difference represents the electromotive force of the process (i.e., how "intense" the movement of charged species is) [44]. The energy densities of systems with different pore sizes and potential windows at 10 mV s^{-1} were calculated using equation (4), and the results obtained were compiled in Fig. 12.

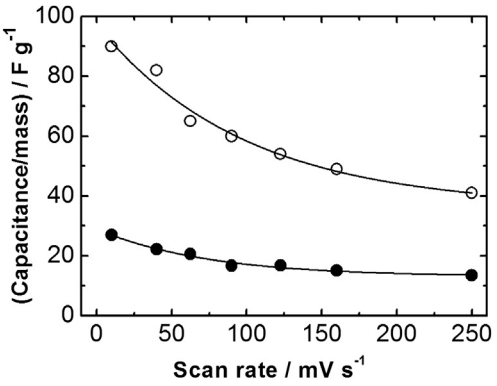

Fig. 10. Initial discharge capacitance as a function of scan rate for 460-nm (pore size) manganese oxide macroporous films. Internal reference = Fc/Fc^+; counter electrode = Pt mesh; electrolytes = [BMMI][Tf_2N] (●) and Li/[BMMI][Tf2N] (○).

$$E = CV^2 \quad (4)$$

where C is the capacitance and V is the electrochemical window.

The positive influence on energy density resulting from enlargement of the potential is clearly observed in the results obtained using both electrolytes, with improvements of up to 75% in the system using the 300-nm macroporous film and Li^+/[BMMI][Tf_2N] as the electrolyte.

The results presented in this study clearly demonstrate the necessity, for any given system, of characterizing and choosing the most suitable IL-based electrolyte to obtain the best performance in terms of capacitance and electrochemical stability throughout successive charge/discharge cycles. The results obtained using

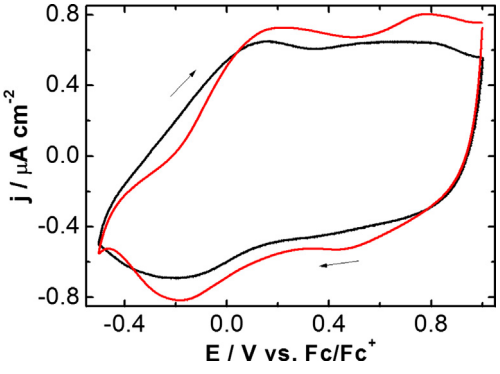

Fig. 11. Cyclic voltammograms of 800-nm (pore diameter) manganese oxide film. Counter-electrode = Pt mesh; internal reference = Fc/Fc^+; scan rate = 0.04 V s^{-1}; electrolytes : Li/[BMMI][Tf_2N] (▪) and Li/PC (●).

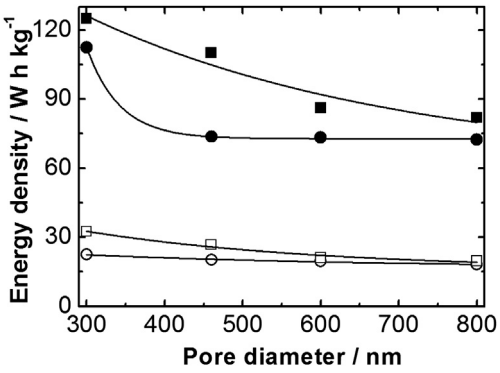

Fig. 12. Energy density as a function of manganese oxide film pore diameter. Scan rate : 0.01 V s^{-1}; internal reference: Fc/Fc^{+}; counter electrode : Pt wire; electrolytes : Li/[BMMI][Tf_2N] (squares) and Li/PC (circles); electrochemical window: 0.9 V (open) and 1.5 V (full).

Li^{+}/[BMMI][Tf_2N] as the electrolyte are interesting, especially when one considers the capacitance values presented in the few published studies regarding the use of manganese oxide films and IL-based electrolytes in supercapacitors [9,45]. Thus, more studies are clearly warranted in this promising field.

4. Conclusions

Macroporous films of manganese oxide were produced by electrodeposition over templates composed of polystyrene spheres with different diameters. With the exception of the 300-nm (pore diameter) film, films with similar surface areas were obtained independent of sphere size when the same amount of material was deposited. The macroporous films obtained were electrochemically characterized by cyclic voltammetry in four different ILs and in propylene carbonate-based electrolytes. The electrochemical behavior of each film, particularly regarding stability throughout successive charge/discharge cycles, was strongly affected by the physico–chemical nature of the IL used. The best performance was obtained when Li^{+}/[BMMI][Tf_2N] was used as the electrolyte; in this case, the capacitance increased until the 700th cycle and then remained constant until at least the 1,000th cycle, achieving values higher than the those obtained when the electrolyte was organic-solvent based. Even at scan rates as high as 250 mV s^{-1}, adding lithium salt to the system caused higher capacitance values, an important consideration with regard to this method's application as an electrochemical capacitor. Widening the electrochemical window to 0.6 V increased the energy density as much as 75%; values as high as 115 Wh kg^{-1} were obtained at 10 mV s^{-1} for the 300 nm (pore diameter) film in Li^{+}/[BMMI][Tf_2N] (as electrolyte). This result, together with the excellent stability throughout cycling under these conditions, makes this system a promising electrochemical capacitor.

Acknowledgments

Financial support was provided by FAPESP (2011/15159-0, 2012/02117-0 and 2009/53199-3), INCT in Bioanalytics (FAPESP, Grant 08/57805-2) and CNPq. Authors would like to thank the Smart Materials Research Center of the University of São Paulo.

Appendix A. Supplementary data

Supplementary data related to this article can be found at http://dx.doi.org/10.1016/j.jpowsour.2013.03.075.

References

[1] M. Armand, F. Endres, D.R. MacFarlane, H. Ohno, B. Scrosati, Nat. Mater. 8 (2009) 621–629.
[2] A. Fernicola, B. Scrosati, H. Ohno, Ionics 12 (2006) 95–102.
[3] V. Borgel, E. Markevich, D. Aurbach, G. Semrau, M. Schmidt, J. Power Sources 189 (2009) 331–336.
[4] T.M. Benedetti, F.F.C. Bazito, E.A. Ponzio, R.M. Torresi, Langmuir 24 (7) (2008) 3602–3610.
[5] W.G. Menezes, D.M. Reis, T.M. Benedetti, M.M. Oliveira, J.F. Soares, R.M. Torresi, A.J.G. Zarbin, J. Colloid Interface Sci. 337 (2009) 586–593.
[6] T.M. Benedetti, E. Redston, W.G. Menezes, D.M. Reis, J.F. Soares, A.J.G. Zarbin, R.M. Torresi, J. Power Sources 224 (2013) 72–79.
[7] H. Ohno, Electrochemical Aspects of Ionic Liquids, Cap 1, John Wiley & Sons, 2011, p. 2005.
[8] J.-K. Chang, M.-T. Lee, W.-T. Tsai, M.-J. Deng, I.-W. Sun, Chem. Mater. 21 (2009) 2688–2695.
[9] J.-K. Chang, M.-T. Lee, C.-W. Cheng, W.-T. Tsai, M.-J. Deng, Y.-C. Hsieh, I.-W. Sun, J. Mater. Chem. 19 (2009) 3732–3738.
[10] M. Anouti, L. Timperman, M. el hilali, A. Boisset, H. Galiano, J. Phys. Chem. C 116 (2012) 9412–9418.
[11] Yun-Shan Li, I.-Wen Sun, Jeng-Kuei Chang, Chung-Jui Su, Ming-Tsung Lee, J. Mater. Chem. 22 (2012) 6274–6279.
[12] H.Y. Lee, J.B. Goodenough, J. Solid State Chem. 144 (1999) 220–223.
[13] W. Wei, X. Cui, W. Chen, D.G. Ivey, Chem. Soc. Rev. 40 (2011) 1697–1721.
[14] H. Gao, F. Xiao, C.B. Ching, H. Duan, ACS Appl. Mater. Interfaces 4 (2012) 2801–2810.
[15] D. Yan, Z. Guo, G. Zhu, Z. Yu, H. Xu, A. Yu, J. Power Sources 199 (2012) 409–412.
[16] J.-L. Liu, L.-Z. Fan, X. Qu, Electrochim. Acta 66 (1) (2012) 302–305.
[17] S. Bach, J.P. Pereira-Ramos, P. Willmann, Electrochim. Acta 56 (27) (2011) 10016–10022.
[18] Y.-C. Lee, T.-J. Kuo, C.-J. Hsu, Y.-W. Su, C.-C. Chen, Langmuir 18 (2002) 9942–9946.
[19] R. Szamocki, A. Velichko, C. Holzapfel, F. Mucklich, S. Revaine, P. Garrigue, N. Sojic, R. Hempelmann, A. Kuhn, Anal. Chem. 79 (2007) 533–539.
[20] X. Luo, A.J. Killard, A. Morrim, M.R. Smith, Chem. Commun. (Cambridge) 30 (2007) 3207–3209.
[21] M. Nakayama, T. Kanaya, R. Inoue, Electrochem. Commun. 9 (2007) 1154–1158.
[22] T.M. Benedetti, V.R. Gonçales, D.F.S. Petri, S.I. Córdoba de Torresi, R.M. Torresi, J. Braz. Chem. Soc. 21 (2010) 1704–1709.
[23] F.F.C. Bazito, Y. Kawano, R.M. Torresi, Electrochim. Acta 52 (2007) 6427–6437.
[24] M.J. Monteiro, F.F. Camilo, M.C.C. Ribeiro, R.M. Torresi, J. Phys. Chem. B 114 (2010) 12488–12494.
[25] G.A. Snook, A.S. Best, A.G. Pandolfo, A.F. Hollenkamp, Electrochem. Commun. 8 (2006) 1405–1411.
[26] C. Gabrielli, M. Keddam, R.M. Torresi, J. Electrochem. Soc. 138 (1991) 2657–2660.
[27] M. Nakayama, T. Kanaya, J.-W. Lee, B.N. Popov, J. Power Sources 179 (2008) 361–366.
[28] H. Malankar, S.S. Umare, K. Singh, J Appl. Electrochem. 40 (2010) 265–275.
[29] P.N. Bartlett, J.J. Baumberg, S. Coyle, M.E. Abdelsalam, Faraday Discuss. 125 (2004) 117–132.
[30] P.N. Bartlett, J.J. Baumberg, P.R. Birkin, M.A. Ghanem, M.C. Netti, Chem. Mater. 14 (2002) 2199–2208.
[31] P.N. Bartlett, P.R. Birkin, M.A. Ghanem, Chem. Commun. 17 (2000) 1671–1672.
[32] V.R. Gonçales, M.P. Massafera, T.M. Benedetti, D.G. Moore, S.I. Córdoba de Torresi, R.M. Torresi, J. Braz. Chem. Soc. 20 (4) (2009) 663–673.
[33] G. Sauerbrey, Z Phys. 155 (1959) 206–222.
[34] P.N. Bartlett, P.R. Birkin, M.A. Ghanem, C. Toh, J. Mater. Chem. 11 (2001) 849–853.
[35] R. Szamocki, A. Velichko, F. Muucklich, S. Reculusa, S. Ravaine, S. Neugebauer, W. Schuhmann, R. Hempelmann, A. Kuhn, Electrochem. Commun. 9 (2007) 2121–2127.
[36] T. Brousse, M. Toupin, R. Dugas, L. Athouel, O. Crosnier, D. Bélanger, J. Electrochem Soc. 153 (12) (2006) A2171–A2180.
[37] K.-W. Nam, C.-W. Lee, X.-Q. Yang, B.W. Choc, W.-S. Yoon, K.-B. Kim, J. Power Sources 188 (2009) 323–331.
[38] G.G. Amatucci, C.N. Schmutz, A. Blyr, C. Sigala, A.S. Gozdz, D. Larcher, J.M. Tarascon, J. Power Sources 69 (1997) 11–25.
[39] M.M. Thackeray, P.J. Johnson, L.A. de Picciotto, Mat. Res. Bull. 19 (1984) 179–187.
[40] J.D. Lee, Concise Inorganic Chemistry, Cap 23, Chapman & Hall, 1996.
[41] R.J. Gummow, A. de Kock, H.M. Thackeray, Solid State Ionics 69 (1994) 59–67.
[42] K. Abe, Y. Ushigoe, H. Yoshitake, M. Yoshio, J. Power Sources 153 (2006) 328–335.
[43] J. Liu, A. Manthiram, Chem. Mater. 21 (2009) 1695–1707.
[44] M. Winter, R.J. Brodd, Chem. Rev. 104 (2004) 4245–4270.
[45] M.-T. Lee, W.-T. Tsai, M.-J. Deng, H.-F. Cheng, I.-W. Sun, J.-K. Chang, J. Power Sources 195 (3) (2010) 919–922.